2022-02-01

Wave energy extraction from a floating flexible circular plate

Michele, Simone

10.1016/j.oceaneng.2021.110275
Ocean Engineering
Elsevier

Title:
Wave energy extraction from a floating flexible circular plate

Journal:
Ocean Engineering

Author names and affiliations:
S. Michele[a], S. Zheng[a,*] and D. Greaves[a]

a School of Engineering, Computing and Mathematics, University of Plymouth, Drake Circus, Plymouth PL4 8AA, United Kingdom

* Email address for correspondence: siming.zheng@plymouth.ac.uk

Received at Editorial Office: 2 Sep 2021
Article revised: 9 Nov 2021
Article accepted for publication: 26 Nov 2021

Wave energy extraction from a floating flexible circular plate

S. Michele[a], S. Zheng[a,*] and D. Greaves[a]

[a]University of Plymouth, Drake Circus, Plymouth, PL4 8AA, Devon, United Kingdom

ARTICLE INFO

Keywords:
Wave energy
Flexible wave energy converters
Fluid-structure interaction

ABSTRACT

We present a theoretical model to investigate the hydrodynamics of a floating flexible circular wave energy converter (WEC). Decomposition in rigid and bending elastic modes of the plate allows us to investigate power extraction efficiency in monochromatic incident waves. We show that plate elasticity increases the number of eigenfrequencies, which has a positive beneficial effect on power output. We also show how plate radius and power take-off (PTO) distribution affect the response of the system and the consequent absorbed energy. This work highlights the need to extend theoretical studies and experimental investigations on flexible devices, currently seen as the future of WEC technology.

1. Introduction

Ocean waves are huge untapped renewable energy resources. A large number of wave energy conversion concepts have been proposed since the 1790s [5]. In recent decades, due to the energy crisis and climate change, wave power has received more attention and has been developed faster than before. In spite of this, the levelised cost of energy (LCOE) of wave energy converters (WECs) is still high, and wave energy has struggled to have the same success as other renewable energies, such as solar and wind power [6].

One of the effective ways to increase the LCOE of WECs is to enhance their wave power absorption efficiency. It has long been known that there is a theoretical limit for wave power absorption by axisymmetric WECs operating in rigid-body motion [e.g., see 2, 7]. For an axisymmetric WEC capturing wave power due to heave motion in regular waves, the theoretical limit of the wave power capture width, which is defined as the absorbed wave power with respect to that contained in a unit length of an incident wave crest, is equivalent to $\lambda/(2\pi)$, where λ denotes the wavelength. For the device capturing wave power through surge and/or pitch motions, the wave power capture width doubles to λ/π. The power capture width can be further increased to $3\lambda/(2\pi)$ should both heave and surge/pitch be adopted for wave power absorption. Very recently, [28] proposed that it was theoretically possible to extend the capture width for axisymmetric WECs without bound through the use of generalised (non-rigid-body) modes of motion. They reported that a vertical cylinder, whose surface is surrounded by an array of narrow vertical absorbing paddles, could achieve well in excess of the standard limit of a capture width of $3\lambda/(2\pi)$ for rigid-body motion, and for some specified wave conditions, the capture width could be as large as $4\lambda/\pi$.

Compared with the conventional rigid-body-based WECs, the WECs made from flexible materials are not only advantageous for the larger potential of wave power absorption but also believed to offer improved performance/survivability and reduced cost in respect to steel/concrete alternatives. In the last decade, there has been a growing trend towards flexible body WECs, e.g., flexible plate WECs [30], bulge wave devices [8], and SQ devices [11]. A comprehensive overview of the current state of the technology of flexible body WECs can be referred to [31, 6].

Among the different kinds of flexible body WECs, the flexible plate WEC could be one of the most simple and is expected to have a range of potential applications. [19] developed a mathematical model and carried out a series of experiments on a two-dimensional flexible device with the goal of decreasing the LCOE of wave power generation and analyse the corresponding hydrodynamics. [30] analysed the coupled hydro-electromechanic response of a two-dimensional piezoelectric device and showed that the piezoelectric plate can extract sufficient energy for low-power devices, like sensors, LEDs, computers, and wireless routers. Hydrodynamic characteristics of the piezoelectric plate WECs in other circumstances have also been investigated, e.g., a piezoelectric plate WEC mooring on a seabed-mounted/floating breakwater [3, 34], and an offshore disk-shaped piezoelectric plate WEC [33]. The piezoelectric plate

*Corresponding author

simone.michele@plymouth.ac.uk (S. Michele); siming.zheng@plymouth.ac.uk (S. Zheng); deborah.greaves@plymouth.ac.uk (D. Greaves)

ORCID(s): 0000-0001-7124-1619 (S. Zheng)

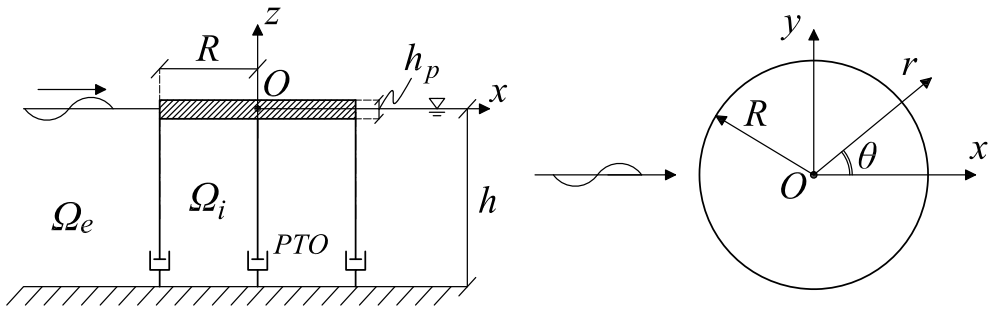

Figure 1: View from above and horizontal cross-section of the flexible circular WEC.

WECs were observed to be effective for a narrow frequency bandwidth. [37, 35, 36] developed theoretical models to study wave interaction with floating/submerged elastic plates and demonstrated profound potential of elastic plates for wave power extraction. It should be pointed out that the power take-off (PTO) system in their work was represented as the porosity of the elastic plates, which is not related to any specified PTO system.

Several studies on floating or submerged circular bodies in waves have already been developed by several authors, with applications in different fields. For example, [16, 17] have recently investigated the motion of a circular elastic plate in the time-domain, theoretical and experimental validations of floating elastic disks to regular waves have been carried out by [26, 25]. Theoretical studies on the scattering of gravity waves by a circular dock are developed in [24, 9], [4] investigated the hydrodynamics of a submerged flexible circular membrane, the case of a circular ice plate has been analysed by [18], [1] applied an integro-differential equation method to study the diffraction of incident surface waves by a floating elastic circular plate, whereas [14] analysed the radiation problem of a heaving submerged disk by applying hypersingular integral equations. [12] constructed a hypersingular integral equation to model the interaction between water waves and plates of small thickness, whereas [10] examined the wave force acting on a circular flexible plate in the presence of a vertical surface-piercing flexible porous membrane.

To the best of our knowledge, applications of elastic circular plates for wave energy extraction have not been well investigated yet. In this paper, a floating elastic circular plate connected to the sea bed through a series of vertical PTO mechanisms is proposed. Compared with the wave power absorption by the "porosity" of elastic plates [37, 35], the PTO system of the present work is much more realistic. It is expected that this device holds a wider frequency bandwidth than the piezoelectric plate WECs [30, 33].To study the performance of the proposed circular flexible WEC, a mathematical model is developed in this paper by means of free-edge dry mode expansion of plate motion [27, 19]. This approach shows explicitly the effects of natural modes on plate motion [29] and is useful to analyse the plate response in detail. The radiation and diffraction velocity potentials in the fluid domain are solved by matching the respective eigenfunctions at the common boundaries [13, 32], whereas the plate response is found by solving for the modal complex amplitudes of each natural mode. Then we derive the theoretical Haskind-Hanaoka relation to check numerical computations [15] and apply the theory to cases of practical interest. We show that plate elasticity has positive effects on power extraction efficiency because of the shifting of bending modes towards smaller frequencies. In particular, rigid plates are much less efficient than flexible devices and are characterised by smaller efficiency bandwidth. Furthermore, we analyse different PTO distributions and plate dimensions and show that they can have both constructive and destructive effects on power extraction.

2. Mathematical model

With reference to Figure 1, consider a floating elastic circular WEC of radius R and small thickness $h_p \ll R$ in open sea of constant depth h. Let us define a Cartesian reference system with the x and y-axes coincident with the undisturbed free-surface level and the z-axis pointing vertically upward. The WEC is connected to the seabed through vertical PTO mechanisms, each with constant damping coefficient ν_{PTO} and located in (r_i, θ_i), $i = 1, ..., I$, where $r = \sqrt{x^2 + y^2}$ represents the radial coordinate and θ is the angular coordinate positive anticlockwise. Since the thickness of the plate is assumed to be much smaller than the radius of the plate R, the elastic vibration of the floater

can be described by the following dynamic equation [29]

$$D\nabla^4 W = q - \rho_p h_p W_{tt}, \quad r \in [0, R], \tag{1}$$

where W represents the plate displacement, t denotes time, q is the transverse distributed load positive in the z-direction, $D = Eh_p^3/12(1-\nu^2)$ represents the flexural rigidity, E is the Young's modulus of the plate material, ν is the Poisson's ratio, ∇^4 denotes the biharmonic operator in cylindrical-polar coordinates, ρ_p is the plate density whereas the subscripts denote differentiation with respect to the relevant variable. For later convenience, let us define the following vertical fluid surface representing the gap under the plate

$$S_f = \{r = R, \theta \in [0, 2\pi], z \in [-h, 0]\}. \tag{2}$$

We assume also inviscid fluid and irrotational flow, hence the velocity potential $\Phi(x, y, z, t)$ satisfies Laplace's equation in the fluid domain $\Omega = \Omega_i \cup \Omega_e$, where Ω_i represents the fluid domain below the plate confined by the surface S_f, whereas Ω_e is the fluid domain for $r > R$. On the free surface, we have the linearised kinematic and mixed boundary conditions

$$\zeta_t = \Phi_z, \quad \Phi_{tt} + g\Phi_z = 0, \quad z = 0, \ r > R, \tag{3}$$

where ζ is the free-surface elevation and g is the acceleration due to gravity. In addition, we require tangential fluid velocity at the seabed

$$\Phi_z = 0, \quad z = -h. \tag{4}$$

By using the thin-plate approximation [13], the kinematic boundary conditions on the wetted surface of the plate reads

$$\Phi_z = W_t, \quad z = 0, \ r \in [0, R]. \tag{5}$$

Since the system is forced by monochromatic incident waves of frequency ω, we assume the following harmonic expansion

$$\{\Phi, \zeta, W\} = \mathrm{Re}\left\{(\phi, \eta, w)e^{-\mathrm{i}\omega t}\right\}, \tag{6}$$

with i being the imaginary unit. We are now ready to write the governing equations in terms of the spatial variables only

$$\nabla^2\phi = 0, \qquad \text{in } \Omega, \tag{7}$$

$$\phi_z = -\mathrm{i}\omega\eta, \qquad z = 0, \ r > R, \tag{8}$$

$$\phi_z = \frac{\omega^2}{g}\phi, \qquad z = 0, \ r > R, \tag{9}$$

$$\phi_z = -\mathrm{i}\omega w, \qquad z = 0, \ r \in [0, R], \tag{10}$$

$$\phi_z = 0, \qquad z = -h, \tag{11}$$

and require the velocity potential ϕ be outgoing for $r \to \infty$. Following [27] and [19], we now decompose the displacement of the device into a set of rigid (heave and pitch) and elastic dry modes, i.e., in the absence of fluid or added mass. By considering incident waves propagating along the x-axis and symmetrical PTO distributions with respect to x, the plate response will show only symmetrical motion. This means that the plate will oscillate only through a combination of axisymmetric modes. Hence

$$w = \zeta_h w_h + \zeta_p w_p + \sum_{m=0}^{\infty}\sum_{n=0}^{\infty} \zeta_{mn} w_{mn}, \tag{12}$$

where ζ_α represents the complex amplitude of each modal shape w_α, heave and pitch modal shapes are simply

$$w_h = 1, \quad w_p = r\cos\theta, \tag{13}$$

whereas the elastic dry mode eigenfunctions are given by the solution of the following boundary value problem [29]

$$D\nabla^4 w_{mn} - \rho_p h_p w_{mn}\omega^2 = 0, \qquad r \in (0, R), \tag{14}$$

$$\frac{\partial^2 w_{mn}}{\partial r^2} + \frac{\nu}{R^2}\frac{\partial^2 w_{mn}}{\partial \theta^2} + \frac{\nu}{R}\frac{\partial w_{mn}}{\partial r} = 0, \qquad r = R, \tag{15}$$

$$\frac{\partial^3 w_{mn}}{\partial r^3} + \frac{2-\nu}{R^2}\frac{\partial^3 w_{mn}}{\partial r \partial \theta^2} + \frac{1}{R}\frac{\partial^2 w_{mn}}{\partial r^2} - \frac{3-\nu}{R^3}\frac{\partial^2 w_{mn}}{\partial \theta^2} - \frac{1}{R^2}\frac{\partial w_{mn}}{\partial r} = 0, \qquad r = R, \tag{16}$$

where conditions (15)-(16) represent zero moment and shear stress at the edge $r = R$, respectively. Separation of variables yields the following solution of the mn-th axisymmetric natural elastic mode

$$w_{mn} = \cos n\theta \left[J_n\left(\frac{\lambda_{mn} r}{R}\right) - I_n\left(\frac{\lambda_{mn} r}{R}\right) T_{mn} \right], \; n = 0, 1, ..., \; m = 0, 1, ... \tag{17}$$

where

$$T_{mn} = \left. \frac{J_n''\left(\frac{\lambda_{mn} r}{R}\right) - \frac{n^2\nu}{R^2} J_n\left(\frac{\lambda_{mn} r}{R}\right) + \frac{\nu}{R} J_n'\left(\frac{\lambda_{mn} r}{R}\right)}{I_n''\left(\frac{\lambda_{mn} r}{R}\right) - \frac{n^2\nu}{R^2} I_n\left(\frac{\lambda_{mn} r}{R}\right) + \frac{\nu}{R} I_n'\left(\frac{\lambda_{mn} r}{R}\right)} \right|_{r=R}, \tag{18}$$

J_n and I_n are the Bessel function and the modified Bessel function of order n, primes indicate the derivative with respect to the radial coordinate r, $\lambda_{mn}^4 = \rho_h h_p R^4 \omega_{mn}^2 / D$ is the root of the eigenvalue condition

$$\begin{aligned} &\left[J_n'' - \frac{n^2\nu}{R^2} J_n + \frac{\nu}{R} J_n' \right]_{r=R} \times \left[J_n''' - \frac{2-\nu}{R^2} n^2 J_n' + \frac{J_n''}{R} + \frac{3-\nu}{R^3} n^2 J_n - \frac{J_n'}{R^2} \right]_{r=R} \\ &- \left[I_n'' - \frac{n^2\nu}{R^2} I_n + \frac{\nu}{R} I_n' \right]_{r=R} \times \left[I_n''' - \frac{2-\nu}{R^2} n^2 I_n' + \frac{I_n''}{R} + \frac{3-\nu}{R^3} n^2 I_n - \frac{I_n'}{R^2} \right]_{r=R} = 0, \end{aligned} \tag{19}$$

whereas ω_{mn} is the relative eigenfrequency. Note that the arguments of the Bessel Functions in (19) are omitted for brevity and that the natural modes w_{mn} satisfy the orthogonal property with respect to the weighting function r, i.e.

$$\int_0^R r \, \mathrm{d}r \int_0^{2\pi} w_{mn} w_{pq} \, \mathrm{d}\theta \neq 0, \quad m = p \wedge n = q. \tag{20}$$

Following the method of [15] we are now in a position to decompose the velocity potential ϕ in diffraction and radiation components, i.e.

$$\phi = \phi_D + \zeta_h \phi_h + \zeta_p \phi_p + \sum_{m=0}^{\infty}\sum_{n=0}^{\infty} \zeta_{mn} \phi_{mn}, \quad \phi_D = \phi_I + \phi_S, \tag{21}$$

where

$$\phi_I = -\frac{\mathrm{i}Ag}{\omega} \sum_{n=0}^{\infty} \epsilon_n \mathrm{i}^n J_n\left(k_0 r\right) \frac{\cosh k_0 (h+z)}{\cosh k_0 h} \cos n\theta, \quad \text{in } \Omega_e, \tag{22}$$

is the incident wave potential expressed in terms of Bessel functions and propagating along the x-axis, A is the amplitude of the incoming waves, the wavenumber k_0 is the real root of the dispersion relation

$$\omega^2 = g k_0 \tanh k_0 h, \tag{23}$$

ϕ_S is the scattering potential, ϕ_D is the diffraction potential satisfying (10) with $w = 0$, ϕ_h is the heaving radiation potential, ϕ_p is the pitching radiation potential, whereas ϕ_{mn} is the radiation potential related to the mn-th elastic mode.

We shall now derive the boundary value problem in each fluid domain. Let $\phi_D^{(i)}$ ($\phi_R^{(i)}$) be the diffraction (radiation) velocity potential in the internal domain Ω_i, and $\phi_D^{(e)}$ ($\phi_R^{(e)}$) be the diffraction (radiation) velocity potential in the external domain Ω_e. The boundary value problem for the fluid domain Ω_e is given by

$$\nabla^2 \phi^{(e)} = 0, \qquad \text{in } \Omega_e, \tag{24}$$

$$g\phi_z^{(e)} - \omega^2\phi^{(e)} = 0, \qquad z = 0,\ r > R, \tag{25}$$

$$\phi_z^{(e)} = 0, \qquad z = -h, \tag{26}$$

$$\phi^{(e)} = \phi^{(i)}, \qquad \text{on } S_f, \tag{27}$$

$$\phi_r^{(e)} = \phi_r^{(i)}, \qquad \text{on } S_f, \tag{28}$$

whereas the boundary value problem for the subdomain Ω_i is governed by

$$\nabla^2\phi^{(i)} = 0, \qquad \text{in } \Omega_i, \tag{29}$$

$$\phi_{D_z}^{(i)} = 0, \qquad z = 0, \tag{30}$$

$$\phi_{R_z}^{(i)} = -\mathrm{i}\omega w, \qquad z = 0, \tag{31}$$

$$\phi_z^{(i)} = 0, \qquad z = -h, \tag{32}$$

and the matching conditions (27)-(28). In the following section we determine the diffraction and radiation velocity potentials in both domains by applying a matched eigenfunction expansion approach.

2.1. Diffraction velocity potential solution

Similarly to [21], the general solution in the external domain reads

$$\phi_D^{(e)} = -\frac{\mathrm{i}Ag}{\omega}\sum_{n=0}^{\infty}\cos n\theta\left\{\frac{\cosh k_0(h+z)}{\cosh k_0 h}\left[\epsilon_n i^n J_n(k_0 r) + \mathcal{A}_{0n}^D\frac{H_n^{(1)}(k_0 r)}{H_n^{(1)\prime}(k_0 r)\Big|_{r=R}}\right] + \sum_{l=1}^{\infty}\mathcal{A}_{ln}^D\frac{K_n(\overline{k_l}r)\cos\overline{k_l}(h+z)}{K_n'(\overline{k_l}r)\Big|_{r=R}\cos\overline{k_l}h}\right\}, \tag{33}$$

where the $\overline{k_l}$'s denote the roots of the dispersion relation related to the evanescent components

$$\omega^2 = -g\overline{k_l}\tan\overline{k_l}h, \tag{34}$$

$H_n^{(1)}$ is the Hankel function of first kind and order n, K_n is the modified Bessel function of second kind and order n, whereas $\mathcal{A}_{ln}$ are unknown complex constants. Similarly, the solution in the fluid domain below the circular plate is given by

$$\phi_D^{(i)} = -\frac{\mathrm{i}Ag}{\omega}\sum_{n=0}^{\infty}\cos n\theta\left\{\mathcal{B}_{0n}^D\left(\frac{r}{R}\right)^n + \sum_{l=1}^{\infty}\mathcal{B}_{ln}^D\frac{I_n(\mu_l r)\cos\mu_l(h+z)}{I_n'(\mu_l r)\big|_{r=R}\cos\mu_l h}\right\}, \quad \mu_l = \frac{l\pi}{h}, \tag{35}$$

where $\mathcal{B}_{ln}^D$ are unknown coefficients. Substituting (33)-(35) in the matching conditions (27)-(28) and integrating over $z \in [-h, 0], \theta \in [0, 2\pi]$, yields an inhomogeneous linear system in the complex constants $\mathcal{A}_{ln}^D$, $\mathcal{B}_{ln}^D$ which can be solved numerically. The detailed numerical procedure, not reported here for brevity, is standard and already present in several papers and textbooks [13, 19].

3. Radiation velocity potential solution

The general solution in Ω_e for each radiation velocity potential α is similar to (33)

$$\phi_\alpha^{(e)} = \sum_{n=0}^{\infty}\cos n\theta\left\{\mathcal{A}_{0n}^\alpha\frac{H_n^{(1)}(k_0 r)\cosh k_0(h+z)}{H_n^{(1)\prime}(k_0 r)\Big|_{r=R}\cosh k_0 h} + \sum_{l=1}^{\infty}\mathcal{A}_{ln}^\alpha\frac{K_n(\overline{k_l}r)\cos\overline{k_l}(h+z)}{K_n'(\overline{k_l}r)\Big|_{r=R}\cos\overline{k_l}h}\right\}, \tag{36}$$

where the term α refers to the heave mode, the pitching mode or the mn-th bending elastic mode. The radiation potential solution in the fluid domain Ω_i is given by the homogeneous part $\phi_{\alpha h}^{(i)}$ and a particular solution that accounts for the plate vibration in $z = 0$. The homogeneous component reads [13]

$$\phi_{\alpha h}^{(i)} = \sum_{n=0}^{\infty}\cos n\theta\left\{\mathcal{B}_{0n}^\alpha\left(\frac{r}{R}\right)^n + \sum_{l=1}^{\infty}\mathcal{B}_{ln}^\alpha\frac{I_n(\mu_l r)\cos\mu_l(h+z)}{I_n'(\mu_l r)\big|_{r=R}\cos\mu_l h}\right\}, \quad \mu_l = \frac{l\pi}{h}, \tag{37}$$

whereas the structure of each particular solution differs from one another. By applying separation of variables, the particular solution for the rigid heave mode is given by [32]

$$\tilde{\phi}_h = -\frac{\mathrm{i}\omega}{2h}\left[z^2 + 2hz - \frac{r^2}{2}\right], \tag{38}$$

the pitching mode yields

$$\tilde{\phi}_p = -\frac{\mathrm{i}\omega r\cos\theta}{8h}\left[4z^2 + 8hz - r^2\right], \tag{39}$$

whereas the particular solution for each bending elastic mode is given by

$$\tilde{\phi}_{mn} = -\mathrm{i}\omega R\frac{\cos n\theta}{\lambda_{mn}}\left\{\frac{\cosh\frac{\lambda_{mn}(h+z)}{R}J_n\left(\frac{\lambda_{mn}r}{R}\right)}{\sinh\frac{\lambda_{mn}h}{R}} + \frac{\cos\frac{\lambda_{mn}(h+z)}{R}I_n\left(\frac{\lambda_{mn}r}{R}\right)}{\sin\frac{\lambda_{mn}h}{R}}T_{mn}\right\}, \quad n = 0, 1, ... \tag{40}$$

and satisfies (17) in $z = 0$. As in the previous section, by matching the velocity potentials in S_f yields a sequence of linear systems in the unknowns $\mathcal{A}^{\alpha}_{ln}$, $\mathcal{B}^{\alpha}_{ln}$ forced by the particular solutions $\tilde{\phi}_h$, $\tilde{\phi}_p$ and $\tilde{\phi}_{mn}$, respectively.

3.1. Plate response and Haskind-Hanaoka relation

Given the effect of all the external forces, the dynamic equation (1) can be expanded as

$$D\nabla^4 W + \rho_p h_p W_{tt} + \rho g W + \left[\sum_{i=1}^{I}\frac{1}{r}\delta\left(r - r_i\right)\delta\left(\theta - \theta_i\right) + \frac{1}{2\pi r}\delta\left(r\right)\right]\nu_{PTO}W_t + \rho\Phi_t = 0, \tag{41}$$

where ρ is the fluid density. The third term represents the hydrostatic pressure, the fourth term denotes the effects of localised forces due to the PTO systems, δ is the Dirac delta function and the last term represents the dynamic pressure exerted by the wave field. Note that the second term in the brackets takes into account a localised force given by a PTO device located in $r = 0$, therefore the Dirac delta function is defined differently. By using both harmonic expansion (6) and dry mode decomposition (12) we get after some straightforward algebra

$$\begin{aligned}
&\sum_{m=0}^{\infty}\sum_{n=0}^{\infty}\zeta_{mn}\left\{w_{mn}\left\{\frac{D\lambda_{mn}^4}{R^4} - \rho_p h_p\omega^2 + \rho g - \mathrm{i}\omega\nu_{PTO}\left[\sum_{i=1}^{I}\frac{1}{r}\delta\left(r - r_i\right)\delta\left(\theta - \theta_i\right) + \frac{1}{2\pi r}\delta\left(r\right)\right]\right\}\right.\\
&\left.-\mathrm{i}\omega\rho\sum_{n=0}^{\infty}\cos n\theta\sum_{m=0}^{\infty}\left\{\mathcal{B}^{mn}_{0n}\left(\frac{r}{R}\right)^n + \sum_{l=1}^{\infty}\mathcal{B}^{mn}_{ln}\frac{I_n(\mu_l r)}{I_n'(\mu_l r)\big|_{r=R}} - \frac{\mathrm{i}\omega R}{\lambda_{mn}}\left[\frac{J_n\left(\frac{\lambda_{mn}r}{R}\right)}{\tanh\frac{\lambda_{mn}h}{R}} + \frac{I_n\left(\frac{\lambda_{mn}r}{R}\right)}{\tan\frac{\lambda_{mn}h}{R}}T_{mn}\right]\right\}\right\}\\
&+\left(\zeta_h w_h + \zeta_p w_p\right)\left\{-\rho_p h_p\omega^2 + \rho g - \mathrm{i}\omega\nu_{PTO}\left[\sum_{i=1}^{I}\frac{1}{r}\delta\left(r - r_i\right)\delta\left(\theta - \theta_i\right) + \frac{1}{2\pi r}\delta\left(r\right)\right]\right\}\\
&-\mathrm{i}\omega\rho\left\{\zeta_h\left[\mathcal{B}^h_{00} + \sum_{l=1}^{\infty}\mathcal{B}^h_{l0}\frac{I_0^{(1)}(\mu_l r)}{I_0^{(1)\prime}(\mu_l r)\big|_{r=R}} + \frac{\mathrm{i}\omega r^2}{4h}\right] + \zeta_p\cos\theta\left[\mathcal{B}^p_{01}\frac{r}{R} + \sum_{l=1}^{\infty}\mathcal{B}^p_{l1}\frac{I_1^{(1)}(\mu_l r)}{I_1^{(1)\prime}(\mu_l r)\big|_{r=R}} + \frac{\mathrm{i}\omega r^3}{8h}\right]\right\}\\
&= Ag\rho\sum_{n=0}^{\infty}\cos n\theta\left\{\mathcal{B}^D_{0n}\left(\frac{r}{R}\right)^n + \sum_{l=1}^{\infty}\mathcal{B}^D_{ln}\frac{I_n(\mu_l r)}{I_n'(\mu_l r)\big|_{r=R}}\right\}.
\end{aligned} \tag{42}$$

The complex modal amplitudes ζ_h, ζ_p and ζ_{mn} can be found by multiplying both sides of (42) by each of the modal shape functions w_α and then integrating with respect the plate wetted surface $r \in [0, R]$, $\theta \in [0, 2\pi]$. The resulting system can be written in the following matrix form

$$\mathbf{M}\left\{\zeta\right\} = \left\{F\right\}, \tag{43}$$

where $\mathbf{M}$ is the coefficient matrix, $\{F\}$ is the exciting force vector, whereas $\{\zeta\}$ is the vector containing the unknown modal amplitudes. For additional details about the numerical procedure above we refer to [13, 19, 27]. As in the case of arrays of WECs, the structure of (43) suggests that the continuous floating plate is equivalent to a system of linear coupled forced harmonic oscillators. Consequently, the natural modes of the WEC coupled with the surrounding fluid are evaluated by equating to zero the determinant of the real components of the coefficient matrix $\mathbf{M}$ [23], i.e.

$$|\mathrm{Re}\,\{\mathbf{M}\}| = 0, \tag{44}$$

which represent all the inertial and stiffness effects. Solution of the latter equation gives the numerical value of each eigenfrequency.

Now, we apply the Haskind–Hanaoka formula to check the numerical computations of the diffraction and radiation velocity potentials. By applying Green's theorem, the expression valid in three-dimensional domains reads [15, 13]

$$F_\alpha = 4\rho k_0^{-1} C_g A \mathcal{A}_\alpha, \tag{45}$$

where the term F_α represents the exciting force given by the following integral

$$F_\alpha = \mathrm{i}\omega\rho \int_0^{2\pi} \mathrm{d}\theta \int_0^R r w_\alpha \, \phi_D^{(i)}\Big|_{z=0} \, \mathrm{d}r, \tag{46}$$

C_g is the group velocity

$$C_g = \frac{\omega}{2k_0}\left(1 + \frac{2k_0 h}{\sinh 2k_0 h}\right), \tag{47}$$

whereas $\mathcal{A}_\alpha$ is the amplitude of radiated waves at large distance from the plate by mode α, for unit modal amplitude and in the direction opposite the incident waves $\theta = \pi$, i.e.

$$\mathcal{A}_\alpha = \sum_{n=0}^{\infty} \frac{\mathrm{i}^n \mathcal{A}_{0n}^R}{H_n^{(1)\prime}(k_0 r)\Big|_{r=R}}, \tag{48}$$

in which $\mathcal{A}_{0n}^R$ represents the first complex coefficient in (36). Theoretical expression (45) relates the diffraction and radiation wave field and is used to perform numerical checks.

3.2. Wave power extraction

Once the response of the system is found, the average generated power by the plate is simply

$$P = \frac{1}{2}\nu_{PTO}\omega^2 \sum_{i=1}^{I} \left| w\left(r_i, \theta_i\right)\right|^2, \tag{49}$$

where $w\left(r_i, \theta_i\right)$ represents the amplitude of plate oscillations corresponding to the PTO location (r_i, θ_i). Then, we measure the system efficiency as the following ratio [15]

$$C_W = \frac{k_0 P}{E C_g}, \quad E = \frac{1}{2}\rho g A^2, \tag{50}$$

where E is the total energy. In the next section we will evaluate the ratio C_W for different plate configurations and PTO distributions.

4. Results and discussion

In this section we examine the effects of plate stiffness, plate geometry and PTO configuration on the hydrodynamic behaviour and energy extraction efficiency. For the sake of example, let us consider the following fixed parameters: $A = 1$ m, $h = 10$ m, $h_p = 1$ m, $\nu = 0.3$ and $\rho = 1000$ kg m^{-3}. Since in the expressions for the velocity potentials and elastic modes there are infinite terms, the summations must be truncated up to a maximum to perform the computations. The convergence analysis performed in Section 4.4 shows that by using $L = 40$ evanescent modes, $N = 5$ angular-terms and the first $M = 5$ dry elastic modes for each n-th component, convergence of the numerical results is reached with good accuracy.

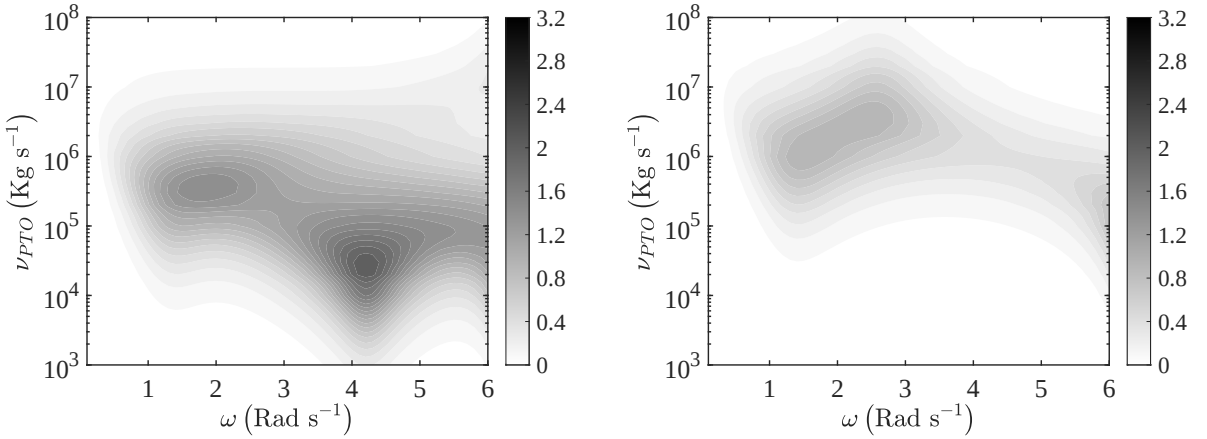

Figure 2: Behaviour of C_W versus frequency of the incident waves ω and PTO-Coefficient ν_{PTO}. (a) 5 PTO devices located in $r = 0$ and $r_i = R, \theta_i = [0, \pi/2, \pi, 3\pi/2]$ rad. (b) Single PTO device located at the center of the plate.

4.1. Effects of the PTO system

In this section we investigate the effects of the PTO coefficient ν_{PTO} and PTO distribution on power extraction efficiency. The Young's modulus of the plate material is $E = 0.1$ GPa, the plate radius is $R = 10$ m, whereas the range of frequency interest is $\omega \in [0.1, 6]$ rad s $^{-1}$. Figure 2 shows the surface plot of the ratio C_W (50) versus incident wave frequency and PTO coefficient for two different PTO distributions. Figure 2(a) refers to the case of five PTO devices located in $r = 0$ and $r_i = R, \theta_i = [0, \pi/2, \pi, 3\pi/2]$ rad, whereas Figure 2(b) shows the case of a single PTO device located at the center of the plate. When the number of the PTOs increases, the bandwidth of C_W increases too and the system also becomes more efficient. This suggest that there could be an optimal distribution of PTO devices maximising power extraction. From a theoretical point of view, this distribution should maximise the radiated waves in the direction opposite the incident waves [15, 13]. Several peaks characterised by values larger than $C_W = 1$ are shown. We remark that this theoretical value corresponds with the maximum of an axis-symmetric WEC in heaving motion [15], therefore plate elasticity and pitching motion further increase power extraction. The fact that multiple degree of freedom WECs are more efficient than rigid devices has also been confirmed in the case of floating elastic plate in two-dimensional domains [19]. Note also that maxima shown in Figure 2(a) are located in correspondence with the first eigenfrequencies of the system, i.e. $\omega = [1.4, 4.2]$ rad s^{-1}. As in the case of oscillating wave surge converters, oscillating water columns and two-dimensional plates, resonance of natural modes is beneficial in terms of power extraction efficiency [20, 19, 21, 22].

Since the PTO system plays a dominant role on the C_W behaviour, we now investigate two additional different configurations, characterised by smaller r_i and greater number of devices, respectively. Figure 3(a) shows the case of a single PTO device in $r = 0$ and a sequence of 8 PTO equally spaced in $r_i = R$, $\theta_i = [0, \pi/4, \pi/2, 3\pi/4, \pi, 5\pi/4, 3\pi/2, 7\pi/4]$. The overall behaviour is similar to that shown in Figure 2(a), except for a larger value of the capture width ratio.

Figure 3(b) shows the case of a PTO device in $r = 0$ and 4 PTO devices in $r_i = R/2, \theta_i = [0, \pi/2, \pi, 3\pi/2]$. The behaviour of C_W shows a single large peak close to the second eigenfrequency $\omega = 4.2$ rad s^{-1} and PTO coefficient $\nu_{PTO} = 3 \times 10^5$ kg s^{-1}. The value of this peak is almost $C_W \sim 2.5$, i.e. larger than the values shown so far. This result further confirms the role of the PTO distribution to maximise power extraction efficiency.

4.2. Effects of plate flexural rigidity

In order to evaluate the effects of plate stiffness on the generated power, a parametric analysis is performed for a softened plate characterised by a smaller value of the Young's modulus $E = 0.05$ GPa and an idealised rigid plate. The 5 PTO devices are located in $r = 0$ and $r_i = R, \theta_i = [0, \pi/2, \pi, 3\pi/2]$ rad whereas the plate radius is $R = 10$ m.

Figure 4(a) shows the case of the softened plate. When the flexural rigidity of the plate decreases, the efficiency of the system increases significantly. This is due to the shifting of the bending mode eigenfrequencies towards smaller frequencies and the fact that these frequencies tend to be much closer one another. Specifically, their numerical values

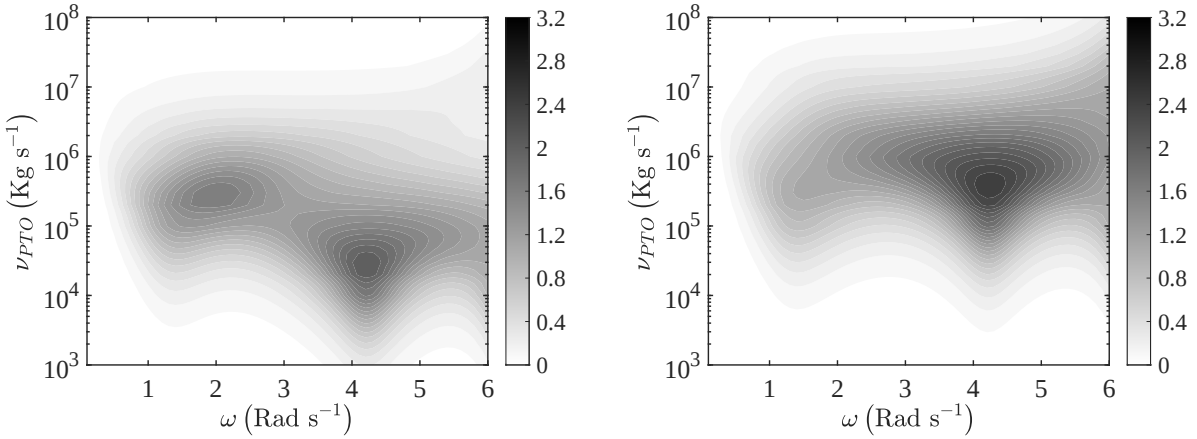

Figure 3: Behaviour of C_W versus frequency of the incident waves and PTO-Coefficient. (a) PTO system characterised by a single PTO device in $r = 0$ and 8 PTO devices equally spaced in $r = R$; (b) The case of 5 PTO devices located in $r = 0$ and $r_i = R/2, \theta_i = [0, \pi/2, \pi, 3\pi/2]$ rad.

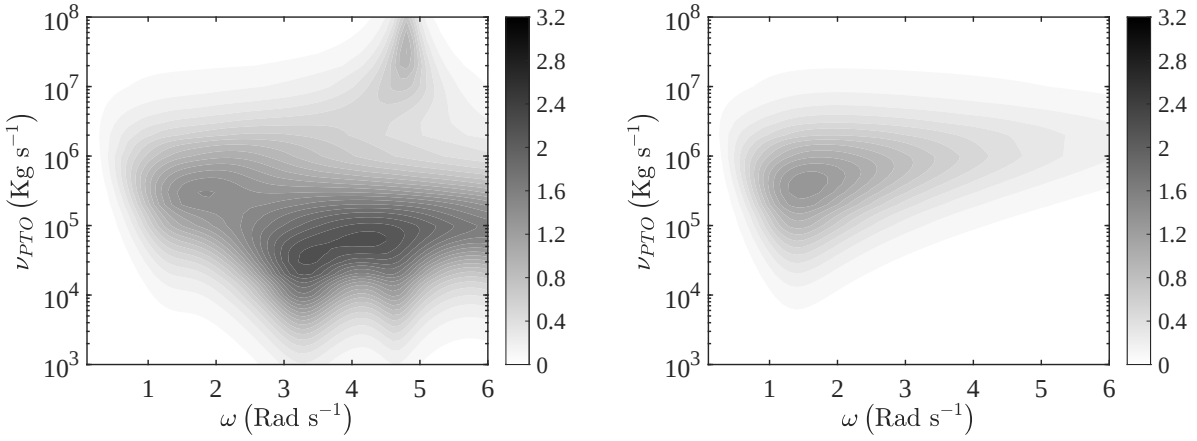

Figure 4: Behaviour of C_W versus frequency of the incident waves and PTO-Coefficient. (a) Flexible plate with Young's modulus $E = 0.05$ GPa; (b) The case of a rigid plate. The 5 PTO devices are located in $r = 0$ and $r_i = R, \theta_i = [0, \pi/2, \pi, 3\pi/2]$ rad.

are now $\omega = [1.4, 3.26, 4.67]$ rad s^{-1}. Differently from the case shown in Figure 2(a), there are now 4 peaks in which the ratio C_W is larger than one. Note that the numerical value of the first eigenfrequency is still unaffected because it represents the eigenfrequency of the rigid mode.

When the plate is rigid, or characterised by very large stiffness, there are no contributions from the bending modes and the dynamics is governed by pitching and heaving motion only. Figure 4(b) shows that there is one maximum around the first eigenfrequency $\omega = 1.4$ rad s^{-1} with value $C_W \sim 1.4$. The overall efficiency is clearly smaller with respect to the cases shown so far because we reduced the number of eigenfrequencies and the resonances of the natural bending modes. Again, this highlights the beneficial effects of the bending elastic modes on power extraction efficiency

4.3. Effects of plate dimensions

Here we investigate the effects given by two different values of plate radius $R = [15; 5]$ m, fixed Young's modulus $E = 0.1$ GPa and fixed PTO distribution. The 5 PTO devices are located in $r = 0$ and $r_i = R, \theta_i = [0, \pi/2, \pi, 3\pi/2]$ rad, i.e. there is one PTO device at the plate center and four equally spaced PTO devices at the plate boundary.

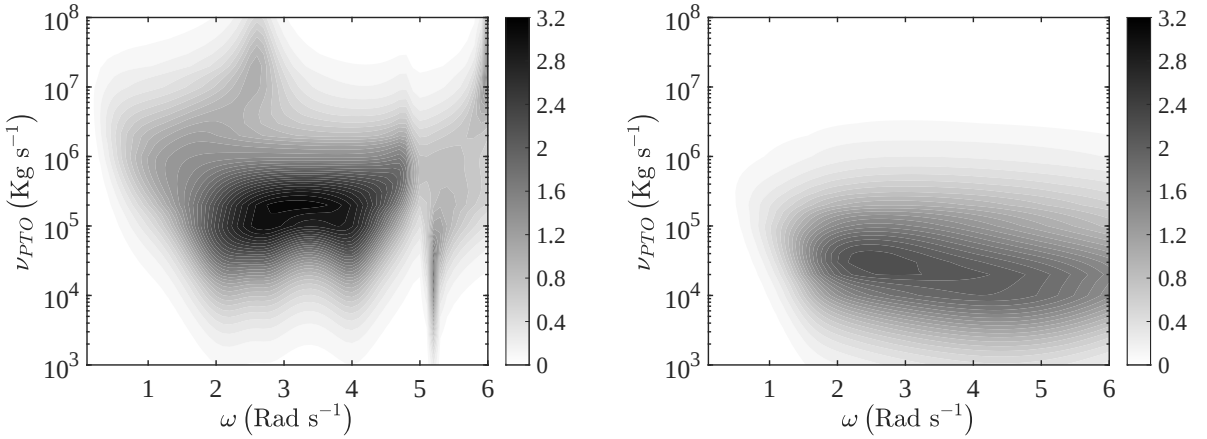

Figure 5: Behaviour of C_W versus frequency of the incident waves and PTO-Coefficient. (a) Plate radius $R = 15$ m; (b) Plate radius $R = 5$ m. The 5 PTO devices are located in $r = 0$ and at the plate boundary $r_i = R, \theta_i = [0, \pi/2, \pi, 3\pi/2]$ rad.

Figure 5(a) shows C_W for the case of larger radius $R = 15$ m. By comparing the same figure with Figure 2(a) we recognise the presence of several additional peaks, larger efficiency bandwidth and also larger values of C_W. This is mainly due to the increased number of eigenfrequencies in the range of interest $\omega = [1.1, 2.1, 2.8, 4.0, 5.1]$ rad s^{-1} which, in addition, are very close to each other. On the contrary, the case of smaller radius $R = 5$ m represented in Figure 5(b), shows smaller overall efficiency with a single visible peak not far from the first eigenfrequency $\omega = 1.8$ rad s^{-1}.

These results suggest that the plate radius R plays an important role on power extraction efficiency, however one should take care of its effects on plate structural resistance that could penalise the overall behaviour and durability in real seas. In fact, larger dimensions mean also larger loads.

4.4. Numerical Convergence Analysis

In this Section we show how the maximum number of vertical eigenfunctions L, angular modes N and radial modes M affects the convergence of numerical results. For the sake of brevity let us assume the case of a single PTO device in $r = 0$ m with damping coefficient $\nu_{PTO} = 10^6$ Kg s^{-1}, Young's modulus of the plate material $E = 0.1$ GPa and plate radius $R = 10$ m. Figure 6 shows the behaviour of C_W versus frequency of incident waves ω for different values of L , N and M. Specifically, Figure 6(a) represents the case of fixed $N = M = 5$ and four values of $L = [10, 20, 30, 40]$, whereas Figure 6(b) represents the case of fixed $L = 40$ and four values of $N = M = [2, 3, 4, 5]$. The same figures show that numerical convergence is reached when: 1) the maximum number of vertical eigenfunctions is $L > 30$; 2) the maximum number of angular and radial bending modes is $(N, M) > 3$. For this reason, in the numerical evaluations above we set $L = 40$ and $N = M = 5$.

5. Conclusions

The purpose of this work is to show how circular flexible devices can be used for wave energy extraction. The mathematical model is based on a linearised potential-flow theory, whereby the method of dry modes is combined with matched eigenfunction expansions, in order to solve the hydrodynamics of radiation and diffraction velocity potentials. The main results of the analytical model show that the effect of the plate elasticity is to increase the number of resonant frequencies with respect to a rigid plate, whereas wave power extraction and the bandwidth of the capture factor become larger. The location of each PTO device plays a significant role, and it is seen that, by increasing the number of PTO devices or modifying the PTO distribution, modal optimisation occurs and the overall efficiency of the system improves. Then we investigated the effect of the plate radius and found that larger plate dimensions yield larger efficiency caused by an increase in the number of resonant frequencies. Given the promising results shown by the mathematical model, our results highlight the need to scale-up experimental investigations on flexible wave energy converters, which are still a small minority, compared to those on rigid converters. An experimental campaign on the

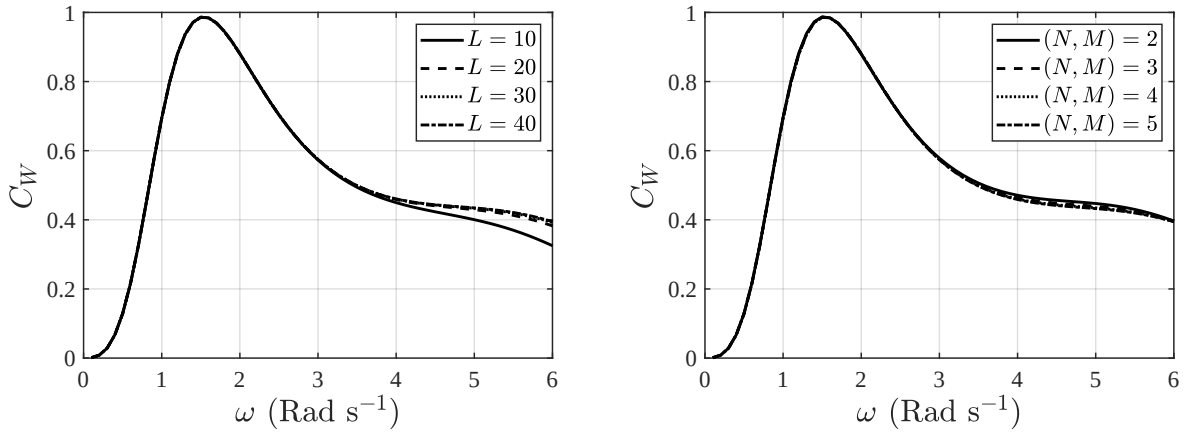

Figure 6: Behaviour of C_W versus frequency of the incident waves for Young's modulus $E = 0.1$ GPa, plate radius $R = 10$ m and single PTO device in $r = 0$ m with fixed coefficient $\nu_{PTO} = 10^6$ kg s^{-1}. (a) Dependence on the maximum number of eigenfunctions for $N = M = 5$; (b) Dependence on the maximum number of bending modes for $L = 40$. The figures above show that numerical convergence can be reached for $L > 30$ and $(N, M) > 3$.

hydrodynamics of a constrained circular flexible disk is being developed. This will allow quantification of the plate response in real seas and in presence of submergence and fluid viscosity.

Funding source

S.M. and S.Z. gratefully acknowledge support from the Supergen ORE Hub ECR Research Fund project ECRRF2021-12 - "Analytical and experimental modelling of a floating/submerged elastic disk". D.G. gratefully acknowledges the EPSRC for supporting part of this work through the Supergen ORE Hub, EP/S000747/1.

References

[1] Adrianov, A.I., Hermans, A.J., 2005. Hydroelasticity of a circular plate on water of finite or infinite depth. J. Fluid Structs. 20, 719–733.
[2] Budal, K., Falnes, J., 1975. A resonant point absorber of ocean waves. Nature 256, 478–479.
[3] Buriani, F., Renzi, E., 2017. Hydrodynamics of a flexible piezoelectric wave energy harvester moored on a breakwater, in: 12th European Wave and Tidal Energy Conference (EWTEC), Cork, Ireland.
[4] Cho, I.H., Kim, M.H., 1999. Wave deformation by a submerged flexible circular disk. Appl. Ocean Res. 21, 263–280.
[5] Clément, A., McCullen, P., Falcão, A.F.d.O., Fiorentino, A., Gardner, F., Hammarlund, K., Lemonis, G., Lewis, T., Nielsen, K., Petroncini, S., Pontes, M.T., Schild, P., Sjöström, B.O., Sørensen, H.C., Thorpe, T., 2002. Wave energy in Europe: current status and perspectives. Renew. Sustain. Energy Rev. 6, 405–431.
[6] Collins, I., Hossain, M., Dettmer, W., Masters, I., 2021. Flexible membrane structures for wave energy harvesting: A review of the developments, materials and computational modelling approaches. Renew. Sustain. Energy Rev. 151, 111478.
[7] Evans, D.V., 1976. A theory for wave-power absorption by oscillating bodies. J. Fluid Mech. 77, 1–25.
[8] Farley, F.J.M., Rainey, R.C.T., Chaplin, J.R., 2012. Rubber tubes in the sea. Philosophical Transactions of the Royal Society A: Mathematical, Physical and Engineering Sciences 370, 381–402.
[9] Garrett, C.J.R., 1971. Wave forces on a circular dock. J. Fluid. Mech. 46, 129–139.
[10] Gayathri, R., Behera, H., 2021. Mitigation of wave force on a circular flexible plate by a surface-piercing flexible porous barrier. Proceedings of the Institution of Mechanical Engineers, Part M: Journal of Engineering for the Maritime Environment 235, 586–599.
[11] Kurniawan, A., Chaplin, J.R., Greaves, D.M., Hann, M., 2017. Wave energy absorption by a floating air bag. J. Fluid Mech. 812, 294–320.
[12] Liang, H., Zheng, S., Shao, Y., Chua, K.H., Choo, Y.S., Greaves, D., 2021. Water wave scattering by impermeable and perforated plates. Phys. Fluids 33, 077111.
[13] Linton, C.M., McIver, P., 2017. Mathematical Techniques for Wave/Structure Interactions. Chapman & Hall/CRC: London, UK.
[14] Martin, P.A., Farina, L., 1997. Radiation of water waves by a heaving submerged horizontal disc. J. Fluid. Mech. 337, 365–379.
[15] Mei, C.C., Stiassnie, M., Yue, D.K.P., 2005. Theory and application of ocean surface waves. World Scientific, Singapore.
[16] Meylan, M.H., 2019. The time-dependent vibration of forced floating elastic plates by eigenfunction matching in two and three dimensions. Wave Motion 88, 21–33.
[17] Meylan, M.H., 2021. Time-dependent motion of a floating circular elastic plate. Fluids 6, 29.

[18] Meylan, M.H., Squire, V.A., 1996. Response of a circular ice floe to ocean waves. J. Geophys. Res. 101, 8869–8884.
[19] Michele, S., Buriani, F., Renzi, E., van Rooij, M., Jayawardhana, B., Vakis, A., 2020. Wave energy extraction by flexible floaters. Energies 13, 6167.
[20] Michele, S., Renzi, E., 2019. A second-order theory for an array of curved wave energy converters in open sea. J. Fluid Structs. 88, 315–330.
[21] Michele, S., Renzi, E., Perez-Collazo, C., Greaves, D., Iglesias, G., 2019a. Power extraction in regular and random waves from an owc in hybrid wind-wave energy systems. Ocean Eng. 191, 106519.
[22] Michele, S., Renzi, E., Sammarco, P., 2019b. Weakly nonlinear theory for a gate-type curved array in waves. J. Fluid Mech. 869, 238–263.
[23] Michele, S., Sammarco, P., d'Errico, M., 2016. The optimal design of a flap gate array in front of a straight vertical wall: resonance of the natural modes and enhancement of the exciting torque. Ocean Eng. 118, 152–164.
[24] Miles, J., Gilbert, F., 1968. Scattering of gravity waves by a circular dock. J. Fluid. Mech. 34, 783–793.
[25] Montiel, F., Bennetts, L.G., Squire, V.A., Bonnefoy, F., Ferrant, P., 2013a. Hydroelastic response of floating elastic discs to regular waves. part 2. modal analysis. J. Fluid. Mech 723, 629–652.
[26] Montiel, F., Bonnefoy, F., Ferrant, P., Bennetts, L.G., Squire, V.A., Marsaul, P., 2013b. Hydroelastic response of floating elastic discs to regular waves. part 1. wave basin experiments. J. Fluid. Mech 723, 604–628.
[27] Newman, J.N., 1994. Wave effects on deformable bodies. Appl. Ocean Res. 16, 47–59.
[28] Porter, R., Zheng, S., Greaves, D., 2021. Extending limits for wave power absorption by axisymmetric devices. J. Fluid Mech. 924, A39.
[29] Reddy, J.N., 2007. Theory and Analysis of Elastic Plates and Shells. CRC Press, Taylor & Francis Group: London, UK.
[30] Renzi, E., 2016. Hydroelectromechanical modelling of a piezoelectric wave energy converter. Proc. R. Soc. A-Math. Phys. 472, 20160715.
[31] Renzi, E., Michele, S., Zheng, S., Jin, S., Greaves, D., 2021. Niche applications and flexible devices for wave energy conversion: A review. Energies 14, 6537.
[32] Yeung, R.W., 1981. Added mass and damping of a vertical cylinder in finite-depth waters. Appl. Ocean Res. 3, 119–133.
[33] Zheng, S., Greaves, D., Meylan, M.H., Iglesias, G., 2020a. Wave power extraction by a submerged piezoelectric plate, in: Developments in Renewable Energies Offshore: Proceedings of the 4th International Conference on Renewable Energies Offshore (RENEW 2020, 12-15 October 2020, Lisbon, Portugal), CRC Press. p. 149.
[34] Zheng, S., Meylan, M., Zhang, X., Iglesias, G., Greaves, D., 2021. Performanceof a plate-wave energy converter integrated in a floating breakwater. IET Renew. Power Gener. 00, 1–14. doi:10.1049/rpg2.12230.
[35] Zheng, S., Meylan, M.H., Fan, L., Greaves, D., Iglesias, G., 2020b. Wave scattering by a floating porous elastic plate of arbitrary shape: a semi-analytical study. J. Fluids Struct. 92, 102827.
[36] Zheng, S., Meylan, M.H., Greaves, D., Iglesias, G., 2020c. Water-wave interaction with submerged porous elastic disks. Phys. Fluids 32, 047106.
[37] Zheng, S., Meylan, M.H., Zhu, G., Greaves, D., Iglesias, G., 2020d. Hydroelastic interaction between water waves and an array of circular floating porous elastic plates. J. Fluid. Mech. 900, A20.